Colloids on the frontier of ferrofluids. Rheological properties

Modesto T. López-López,[1*] Ana Gómez-Ramírez,[1] Laura Rodríguez-Arco,[1] Juan D.G. Durán,[1] Larisa Iskakova,[2] Andrey Zubarev[2]

[1] Department of Applied Physics, University of Granada, Avda. Fuentenueva s/n, 18071, Granada (Spain)

[2] Department of Mathematical Physics, Ural Federal University, Lenin Av. 51, 620083 Ekaterinburg, Russia

Abstract

This paper is devoted to the steady-state rheological properties of two new kinds of ferrofluids. One of these was constituted by CoNi nanospheres of 24 nm in diameter, whereas the other by CoNi nanofibers of 56 nm in length and 6.6 nm in width. These ferrofluids were subjected to shear rate ramps under the presence of magnetic fields of different intensity, and the corresponding shear stress values were measured. From the obtained rheograms (shear stress vs. shear rate curves) the values of both the static and the dynamic yield stresses were obtained as a function of the magnetic field. The magnetoviscous effect was also obtained as a function of both the shear rate and the magnetic field. The experimental results demonstrate that upon magnetic field application these new ferrofluids develop yield stresses and magnetoviscous effects much higher than conventional ferrofluids, based on nanospheres of approximately 10 nm in diameter.

* Corresponding author. Email: modesto@ugr.es

Besides some expected differences, such as the stronger magnetorheological effect in the case of ferrofluids based on nanofibers, some intriguing differences are found between the rheological behaviors of nanofiber ferrofluids and nanosphere ferrofluid. Firstly, upon field application the rheograms of nanofiber ferrofluids present N-shape dependence of the shear stress on the shear rate. The decreasing part of the rheograms takes place at low shear rate. These regions of negative differential viscosity and, therefore, unstable flow are not observed in the case of nanosphere ferrofluids. The second intriguing difference concerns the curvature of the yield stress vs. magnetic field curves. This curvature is negative in the case of nanosphere ferrofluid, giving rise to saturation of the yield stress at medium field, as expected. However, in the case of nanofiber ferrofluid this curvature is positive, which means a faster increase of the yield stress with the magnetic field the higher the magnitude of the latter. These interesting differences may be due to the existence of strong interparticle solid friction in the case of nanofiber ferrofluids. Finally, theoretical models for the static yield stress of the ferrofluids were developed. These models consider that upon field application the ferrofluid nanoparticles are condensed in drops of dense phase. These drops tend to be aligned along the field direction, opposing to the flow of the ferrofluids, and being responsible for the static quasielastic deformation and the yield-stress phenomena. By considering the existence of interparticle dry friction only in the case of nanofiber ferrofluids, the developed models predicted quite well not only the magnitude of the static yield stress, but also the differences in curvature of the yield stress vs. magnetic field curves.

1. Introduction

Magnetic control of the properties and behavior of liquids is a promising field for advanced applications and a challenge for basic research. Since natural liquids react very weakly upon magnetic field application, many efforts of the scientific community have been directed to the development of synthetic fluids that fulfill this goal, commonly known as magnetic fluids. Two main types of magnetic fluids are known since the middle of the twentieth century, magnetorheological (MR) fluids and ferrofluids.[1-4] The former are suspensions of micron-sized particles of magnetizable materials dispersed in a liquid carrier.[5] Particles of this size are magnetically multidomain, which constitutes the physical reason for the distinctive characteristics of MR fluids. In the absence of applied magnetic field, particles of a MR fluid have zero magnetic moment, and consequently there is not magnetic interaction between them. The resulting rheological behavior is this of a suspension of non-magnetic particles, being Newtonian at concentrations far from the maximum packing fraction. On the other hand, when a magnetic field is applied particles of a MR fluid develop a net magnetic moment, which gives rise to strong magnetostatic attraction between particles and to the consequent formation of particle structures aligned with the applied field. These structures hinder the flow of the fluid and, as a consequence, the rheological properties of MR fluids change to those of plastic materials, presenting high values of the yield stress and the viscosity, with intensity dependent on the magnetic field strength. This property, known as MR effect is the base for many applications of MR fluids. A recent review on applications of MR fluids is given in Ref. 6.

On the other hand, according to its most rigorous definition, an ideal ferrofluid is a colloidal suspension of nanoparticles of ferro- or ferrimagnetic materials dispersed in a

liquid carrier that does not settle out, even after long exposure to a force field (gravitational or magnetic).[2] Such definition imposes a restriction to the dispersed particles, which must be smaller than approximately 10 nm in diameter and, besides, coated with a molecular layer of a dispersant that stabilizes against van der Waals attractive forces. Under these conditions, Brownian motion dominates over all other forces of interaction. Effects of applied magnetic fields on the rheological properties of ideal ferrofluids are limited to small increments of their viscosity, which are explained by the hindrance of the free rotation of the particles in a shear flow, as a consequence of the tendency of the magnetic moments (fixed within the particles) to orientate towards the field direction.[7-10]

However, real ferrofluids are polydispersed and a fraction of the particles are large enough so that the dipole-dipole energy of interaction between them overcomes Brownian motion, and thus they cluster upon magnetic field application, which gives rise to moderately high changes of viscosity and even to the appearance of yield stress. In view of this, in practical terms, a ferrofluid may be defined as a suspension of single-domain magnetic particles in a liquid carrier.[10] In this work we will use this definition that, besides being more consistent with reality, allows the classification of magnetic fluids into two categories, MR fluids and ferrofluids. Otherwise, if we consider the rigorous definition of Rosensweig,[2] there is a range of particle sizes (those small enough to be single-domain, but too large for giving rise to an ultrastable colloid) that does not fall into any of the previous categories.

The aim of the present work is precisely to explore the rheological properties of ferrofluids with particle size in this range, which depending on the material goes from 10-15 nm up to 30-40 nm in diameter. To the best of our knowledge, few attempts of studying this range of particle sizes are found in the literature, the work described in Ref. 9 being the most

evident. These authors studied polydispersed ferrofluids having particles up to a maximum diameter of 20 nm. In the present work we will study ferrofluids with even larger particle size, close to the limit of domain breaking. With this aim, spherical CoNi particles of 24 nm in mean diameter will be used. Furthermore, we will study another ferrofluid having fiber-like CoNi particles of 56 nm in length and 6.6 nm in width. Our interest in the use of fiber-like particles for the preparation of ferrofluids has been motivated by previous studies on the field of MR fluids, where the use of non-spherical microparticles has proved as an effective way to enhance the MR response.[11-16] In the field of ferrofluids only spherical particles have been used until very recently, the work described in Ref. 17 being, to the best of our knowledge, the first in using non-spherical particles –namely disc-like particles.

2. Materials

Spherical and fiber-like nanoparticles of CoNi alloy were synthesized by the polyol method as described in Ref. 18. The characterization of the morphology, chemical composition, crystal structure and magnetic properties of these particles is presented in details in Ref. 18. For the purpose of the present work, only the size, shape and magnetic properties of the particles are relevant. As an example, TEM pictures of these particles are shown in Figure 1. From pictures like these of Figure 1, the size of the particles was obtained. The spherical particles have a mean diameter of 24 ± 3 nm, whereas the fiber-like particles have mean length and width of 56 ± 15 nm and 6.6 ± 1.1 nm, respectively.

The saturation magnetization of the CoNi materials is 742.5 ± 0.8 kA m^{-1} and 626 ± 2 kA m^{-1} for spheres and fibers, respectively. The higher saturation magnetization of nanospheres is due to their higher cobalt content with respect to nanofibers.[18] Note that the critical

diameter for magnetically single-domain spherical particles is 30 nm for Fe and larger for Co and Ni.[19] Therefore, the spherical CoNi particles considered in this work are definitely single-domain particles, as derived from the general theory of the magnetic properties of fine particles.[19] Nevertheless, they are large enough to have their magnetic moment fixed in the direction dictated by crystal anisotropy –the critical diameter for intrinsic superparamagnetism is around 10 nm for ferromagnetic particles.[2] Besides, the critical single-domain volume for acicular particles is greater than that for a spherical particle of the same material, since there is less energy to be gained by introducing a domain wall because a larger aspect ratio reduces the magnetostatic energy.[20] Thus, it can also be concluded that the fiber-like CoNi particles considered in this work are also single-domain particles. For one of these nanofibers, the magnetic moment will be along its axis of symmetry.[20]
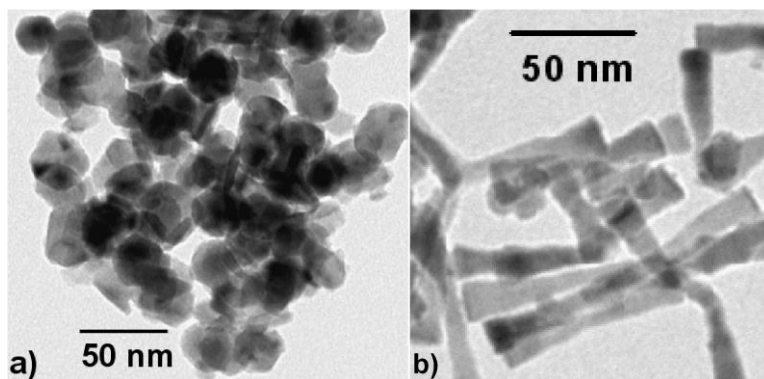

Figure 1. TEM pictures of the spherical (a) and the fiber-like (b) nanoparticles used in this work.

The ferrofluids were prepared by dispersing proper amounts of the synthesized powders in a mineral oil of viscosity 39.58 ± 0.16 mPa·s at 25 ºC (Fluka). L-α-phosphatidylcholine (Sigma-Aldrich, BioChemika) was used as surfactant to avoid irreversible particle

aggregation. Particle concentration was 5 vol.% in all cases –note that this is the usual particle concentration in conventional ferrofluids.

3. Magnetic properties, sedimentation behavior and field-induced structuration of the ferrofluids

3.1. Magnetic properties

The magnetization, M, of the ferrofluids was measured at 25 ºC as a function of the magnetic field strength, H, in a Squid Quantum Design MPMS XL magnetometer (Quantum Design, USA). The results obtained are shown in Figure 2.
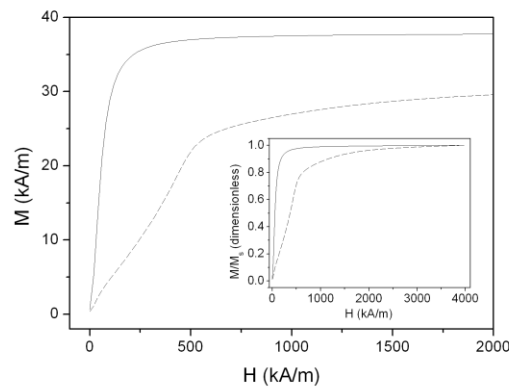

Figure 2. Magnetization of ferrofluids (M) plotted as a function of the applied field strength (H). The continuous and discontinuous lines represent respectively the data for ferrofluids composed of nanospheres (24 nm in diameter) or nanofibers (56 nm in length, 6.6 nm in width). The inset shows the magnetization normalized by the saturation magnetization of the ferrofluid (Ms).

From the values of the saturation magnetization of the ferrofluids (37.9 kA/m and 30.7 kA/m respectively for nanosphere and nanofiber ferrofluids) and those of the dry powders, we obtain volume concentrations of solids of 5.1 % and 4.9 % for nanosphere ferrofluid and nanofiber ferrofluid, respectively. The observed higher saturation magnetization of the

7

ferrofluid composed of nanospheres is thus mainly due to the higher Co content of the nanospheres as compared with nanofibers, as mentioned in the previous section. Besides, the magnetic susceptibility at low and medium field is higher for the ferrofluid composed of nanospheres than for the one composed of nanofibers. This is best observed if the magnetization is normalized by the saturation magnetization, as shown in the inset of Figure 2. This behavior could be due to the smaller volume of the nanofibers as compared with the nanospheres, as well as to the orientation of the nanofibers with respect to the applied field, which may have an important effect on the demagnetizing field and, therefore, on the internal field that determines the state of magnetization of the samples. As will be discussed in the next subsection, a concentration of 5 vol.% is close to that required for a concentrated isotropic regime, in which the free movement of the nanofibers is hindered by contacts with neighboring ones, which could prevent from a perfect alignment of the nanofibers with the applied magnetic field. As a conclusion, it can be said that the ferrofluid composed of nanofibers presents weaker magnetic properties than the one composed of nanospheres.

3.2. Sedimentation behavior

The nanofiber ferrofluid (solid concentration 5 vol.%) was stable and did not experience any kind of phase separation even after 6 months of preparation. On the other hand, in the case of the nanosphere ferrofluid, there was a thin supernatant after a few days of preparation. Similar results were found when the ferrofluids were placed on a powerful magnet (500 mT) for 1 day: nanofiber ferrofluid did not experience phase separation, whereas a sediment was observed in the case of nanosphere ferrofluid.

In order to have quantitative data on the settling behavior of the nanofibers and the nanospheres, we monitored the time evolution of the optical absorbance of diluted suspensions (dilution ratio 1:50 as compared with the original ferrofluids containing 5 vol.% of particles). With this aim, a Milton Roy spectrophotometer (model Spectronic 601, USA) at wavelength $\lambda = 550$ nm was used. The suspensions were poured in square cuvettes with 1 cm light path; the center of the light beam strikes the cuvette 1.5 cm above its bottom. Results of absorbance experiments are shown in Figure 3.
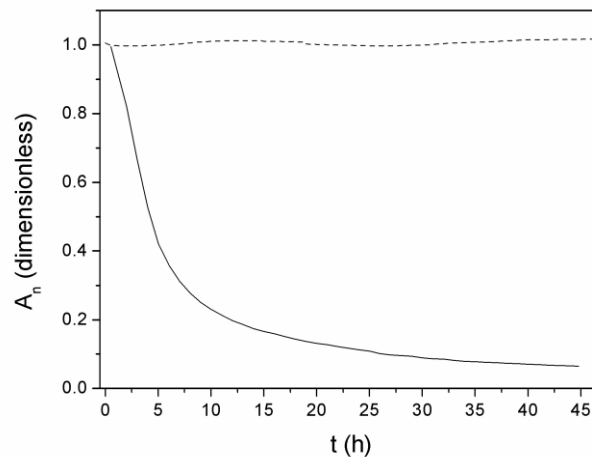

Figure 3. Normalized absorbance A_n (A/A_0) vs time for diluted ferrofluids. Dilution ratio 1:50 as compared with the original ferrofluids containing 5 vol.% of particles. The continuous and discontinuous lines represent respectively the data for ferrofluids composed of nanospheres or nanofibers.

As observed, nanospheres present a clear tendency to settle, whereas nanofibers remain in suspension for the whole time of the experiment, in agreement with observations in more concentrated ferrofluids (5 vol.%). The likely reason for this different behavior is the higher mean volume of nanospheres (7200 nm^3) with respect to nanofibers (1900 nm^3), which probably makes Brownian motion insufficient to stabilize nanospheres against gravitational settling, whereas it seems to be enough in the case of nanofibers. Additionally, for the

9

nanofiber ferrofluid containing 5 vol.% of solids, the stability against settling should also benefit from the fact that this concentration (5 vol.%) is close to the onset of the concentrated isotropic regime, in which the fibers begin to have difficulty packing isotropically because of excluded-volume interactions.[21] This regime is obtained for an approximate concentration given by the following equation:[21]

$$\phi \approx \pi/4p \qquad (1)$$

In this equation ϕ and p stand for the volume fraction of fibers and their aspect ratio, respectively. Taking into account that $p = 8.5$ we obtain $\phi \approx 9$ vol.% for the nanofibers of the present work. Consequently, the nanofiber ferrofluid with concentration 5 vol.% is in a regime in which excluded-volume interactions likely play an important role, involving an additional hindrance to particle settling. At this point, it is important to note that in the case of diluted samples (1:50 with respect to ferrofluids containing 5 vol.% of particles), it was possible to induce phase separation by placing the samples on a powerful magnet, even in the case of nanofibers. Therefore, the ultrastability observed for the nanofiber ferrofluid containing 5 vol.% of particles must have its main origin in the high concentration of fibers, which hinders settling.

3.3. Field-induced structuration of the ferrofluids

One of the hypotheses that will be used in the next section for the interpretation of the rheological properties of the ferrofluids studied in this work is the existence of magnetic field-induced particle structures. In order to corroborate this hypothesis we made observations of diluted ferrofluids upon magnetic fields by using a Nikon SMZ800 optical microscope (Japan). For this aim the ferrofluid samples were squeezed between two glass

slides and magnetic fields were applied with the help of a coil (field parallel to the axis of the microscope) or a pair of Helmholtz coils (field perpendicular to the axis of the microscope). Although the direct observation of the nanoparticles (both fibers and spheres) was impossible, we were able to confirm the existence of field-induced particle structures in both ferrofluids. As an example, Figure 4 shows some photographs of the structures observed upon magnetic field application.
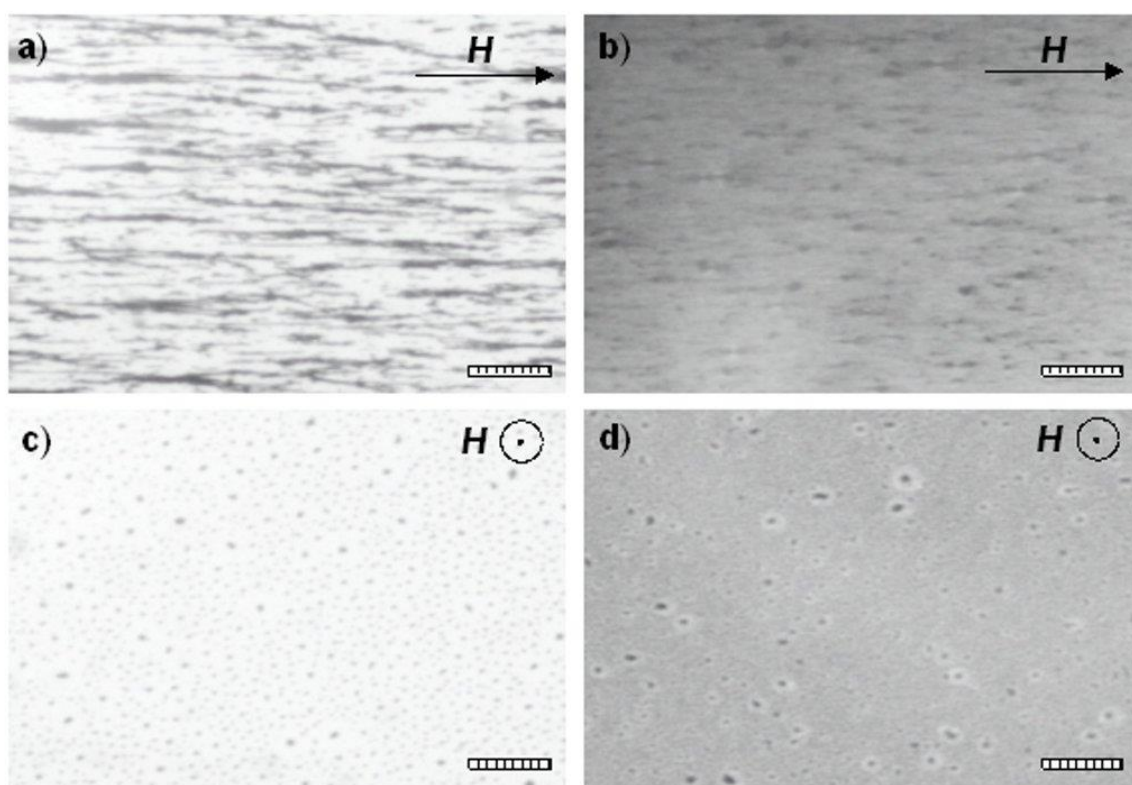

Figure 4. Photos of structures in diluted ferrofluid (1:10 with respect to ferrofluids containing 5 vol.% of particles) confined between two parallel glass slides (the gap was fixed to 0.15 mm). a) and c) correspond to nanosphere ferrofluid; b) and d) to nanofiber ferrofluid; a) and b) were taken upon a field of 9.8 kA/m perpendicular to the axis of the microscope; c) and d) upon a field of 64 kA/m parallel to the axis of the microscope. Bar length: 100 microns.

As can be seen in Figures 4a and 4b particle structures were induced in both ferrofluids. Nevertheless, these are more evident in the case of nanosphere ferrofluid, where all the particles seem to contribute to the field-induced structures. On the other hand, in the case of nanofiber ferrofluid, both the length and width of the particle structures are smaller and, besides, the darker (with respect to nanosphere ferrofluid) and uniform color of the background seems to indicate that an important fraction of the nanofibers remains homogenously distributed, without contributing to the field-induced structures. This may be due to the smaller volume of the nanofibers (with respect to the nanospheres), which makes Brownian motion relatively more important, and thus magnetostatic forces less important, than in the case of nanospheres. Only a small fraction of the nanofibers, consisting of the biggest ones, seems to aggregate upon application of 9.8 kA/m. Figures 4c and 4d were taken upon application of a magnetic field parallel to the axis of the microscope. The black spots observed in both pictures evidence the existence of percolating structures between both glass slides. Again, a darker background is observed in the case of the nanofiber ferrofluid, indicating the existence of a fraction of free (non-aggregated) nanofibers.

4. Rheological properties of ferrofluids

The rheological properties of ferrofluids, both in absence and presence of applied magnetic field, were investigated with a commercial rheometer (MCR 300 Physica Anton Paar, Austria) at a temperature of 25 ºC. The measuring system geometry was a 20 mm diameter parallel-plate set. The gap thickness between both plates was 0.35 mm in all measurements. The magnetic field was generated in the vertical direction with the magnetocell of the rheometer. The magnetic field generated by this magnetocell presents a radial gradient, with a pseudoplateau at medium radial distance.[22,23] The effect of similar field gradients on

the measured shear stress is discussed elsewhere for highly concentrated (46.5 vol.% of iron) MR fluids.[23] Note, however, that in the present work the effect of field gradient is expected to be negligible owing to the relatively weak magnetization of the studied samples. By means of finite element method (FEM) simulation, using the software Finite Element Method Magnetics (FEMM),[24] we calculated the radial distribution of the magnetic field inside the ferrofluids placed in the measuring gap. For this aim we considered an axisymmetric geometry, with the exact dimensions and materials of the real magnetocell of the magnetorheometer MCR 300 Physica Anton Paar. The magnetic properties of the materials of the magnetocell were taken from bibliographic data, and those of the ferrofluid samples from their experimental curves of magnetization (see Figure 2). The values of the internal field strength corresponding to the pseudoplateau at medium radial distance and at 0.175 mm above the bottom plate are plotted as a function of the coil current in Figure 5. These are the values of magnetic field that will be used in this work.

The steady-state shear flow of the ferrofluids was studied for different intensities of the coil current. With this aim, experiments were performed as follows. The ferrofluid was placed in the measuring system of the rheometer and pre-sheared for 30 s at 35 s^{-1} in order to ensure equal initial conditions. Then, an electric current was applied to the magnetocell and 30 s were allowed in the absence of shear so that the sample could be structured before the measurement. Immediately afterwards, and with the same coil current than in the previous step, the ferrofluid was subjected to a shear rate ($\dot{\gamma}$) ramp (up to 175 s^{-1}) and the corresponding shear stress (τ) was measured. Each value of the shear rate was maintained during 10 s. This protocol was carried out for coil currents in the range 0-2 A (see Figure 5 for the corresponding magnetic field strength inside the ferrofluids).
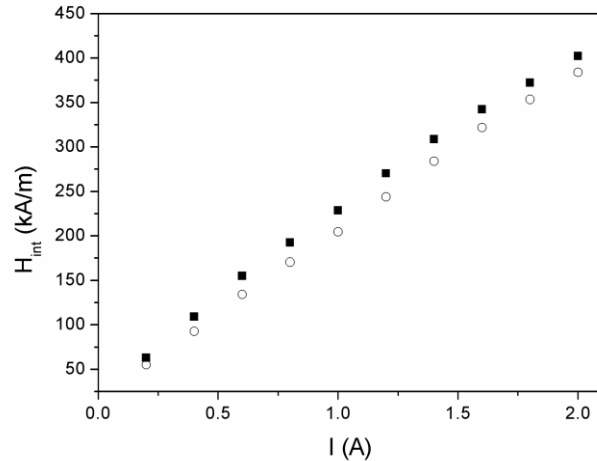
Figure 5. Internal magnetic field (H_{int}) for ferrofluids placed in the measuring gap as a function of the electric current (*I*) flowing through the coil of the magnetocell of the MCR 300 rheometer. The values of the internal field given are those at a radial position 5 mm and at a vertical position 0.175 mm above the lower plate. Calculations were done by FEM simulation. Full squares correspond to the nanofiber ferrofluid; open circles to the nanosphere ferrofluid.

The rheograms (shear stress versus shear rate curves) obtained for the different intensities of the internal magnetic field are shown in Figure 6, for both the ferrofluid composed of nanospheres and the ferrofluid composed of nanofibers. As observed, both ferrofluids present a MR behavior in the presence of magnetic field. This behavior is characterized by the increasing shear stress, for a given shear rate, as the intensity of the magnetic field is increased.[5] In spite of presenting both ferrofluids a MR behavior, the rheograms obtained for the nanofiber ferrofluid are significantly different from those obtained for the nanosphere ferrofluid. The first difference concerns the values of the shear stress reached at the highest magnetic field. These values are even higher than 700 Pa for the nanofiber ferrofluid whereas they are lower than 275 Pa for the nanosphere ferrofluid. This is associated to a stronger MR response in the case of nanofibers, and will be analyzed in details below.
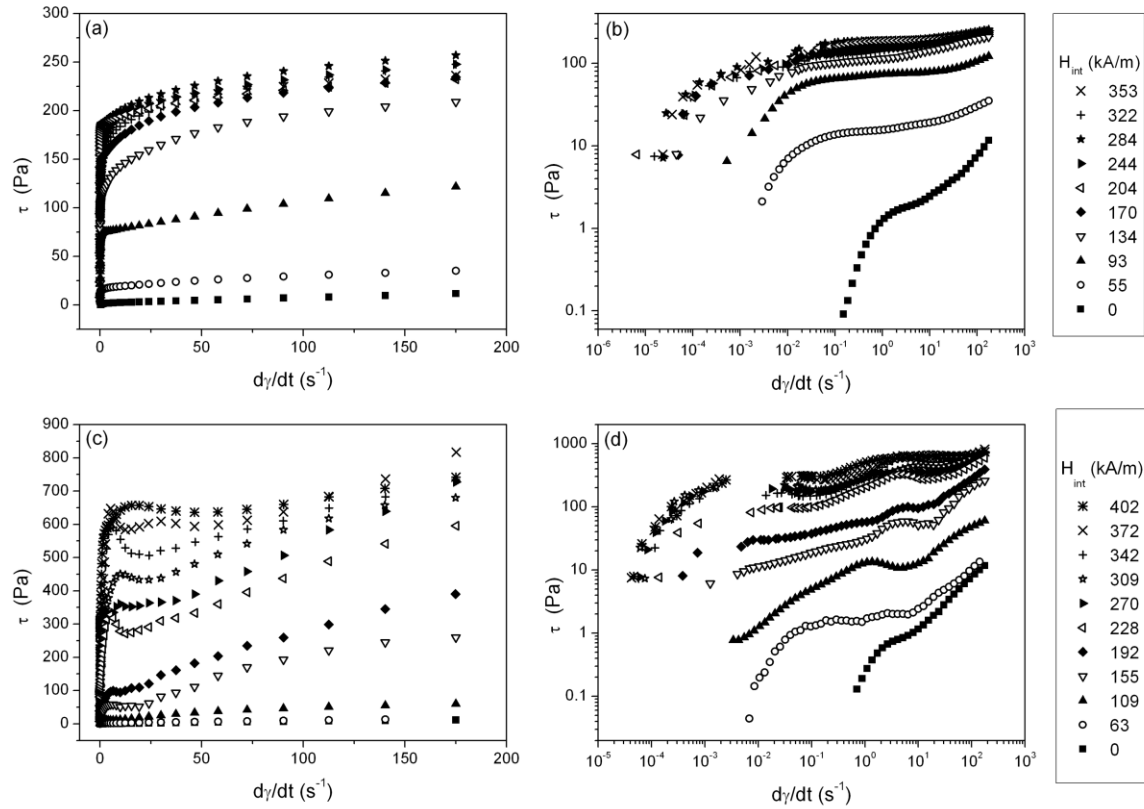
Figure 6. Shear stress (τ) plotted as a function of shear rate ($d\gamma/dt$) for different values of electric current in the magnetocell. The corresponding magnetic field strength inside the ferrofluids (H_{int}) is given. (a) and (b) correspond to curves for the ferrofluid composed of nanospheres; (c) and (d) to curves for the ferrofluid composed of nanofibers.

The second difference is related to the progressive saturation of the response with the internal field. As better observed in Figure 6a, the rheological response of the nanosphere ferrofluid is practically saturated at an internal field of approximately 200 kA/m, i.e. no appreciably ulterior change is obtained by increasing the field. On the other hand, for the nanofiber ferrofluid (see Figure 6c), appreciable changes are observed even for the highest field considered in this study. This could be partially due to the fact that the nanosphere ferrofluid magnetically saturates at a lower field than the nanofiber ferrofluid, as observed in Figure 2, and also to the existence of solid friction between nanofibers as will be discussed in the theoretical section.

The third difference is the N-shape dependence of the shear stress on the shear rate, observed only for the nanofiber ferrofluid. This feature that gives to the rheograms a shape with an overshoot in the shear stress may be explained as follows. As discussed in subsection 3.2, a concentration of 5 vol.% in the case of nanofibers is close to the onset of the concentrated isotropic regime, in which the fibers begin to have difficulty packing isotropically because of excluded-volume interactions. Thus, we may expect that before field application the internal state of the nanofiber ferrofluid is approximately isotropic, but with frequent collisions (excluded-volume interactions) between particles. When a magnetic field is applied, nanofibers will tend to both orientate in the direction of the applied field (to minimize their demagnetizing field) and to aggregate forming particle structures aligned with the field –note that the formation of particle structures in the case of nanofiber ferrofluid was proved by direct microscopic observations (see Figure 4); note also that the magnetic fields applied in rheological experiments are in general stronger than these of Figure 4 and, consequently, a larger fraction of nanofibers is expected to contribute to the field-induced structures. However, in the absence of field contacts between nanofibers should be common due to the rather concentrated regime of the nanofiber ferrofluid. Thus, the consequent friction that must arise when nanofibers tend to move relatively to each other is expected to hinder from a perfect alignment of the nanofibers with the field –note that the nanofibers present a rough, irregular surface, which should favor friction (see Figure 1b). Therefore, we may suppose that at the beginning of the shear rate ramp, nanofibers form entangled, percolating structures. Direct observation of the nanofibers to corroborate the entanglement was not possible due to the nanometric size of the fibers. Nevertheless, this hypothesis was experimentally found to be true for Co microfibers.[12] We think that it may be the same in the case of the CoNi nanofibers used in

this work. We also may suppose that the contact interactions (friction) between the nanofibers prevent from destruction of the particle structures up to a certain (critical) value of the shear rate. When the shear rate achieves this critical value, the destruction of the structures and, therefore, a decrease of the measured shear stress takes place. If all the structures were identical, a sharp decrease of the shear stress at this critical value of the shear rate would be obtained. Afterwards, the ferrofluid would be constituted by relatively short clusters of fibers. Subsequent increase of the shear rate would lead to almost linear increase of the shear stress. However, we experimentally obtained that the rheograms present a smooth shape (see Figure 6c). From our point of view this smooth shape reflects some statistics on the distribution of the initial percolating structures over friction nets of the fibers. Different structures are destroyed at different values of the shear rate and, as a result, smooth rheograms are obtained. A detailed study of this statistics and its effect on the rheological properties of the nanofiber ferrofluids is planned for the future. Note, finally, that since friction between particles of spherical shape is negligible, according to the discussed hypothesis this stress overshoot cannot appear in nanosphere ferrofluids (in agreement with data in Figure 6a).

4.1. Static yield stress

Let us now analyze in more details the MR response of the ferrofluids. The curves of Figure 6 obtained for non-zero magnetic field are typical of a non-ideal plastic behavior, characterized by the existence of a non-negligible value of the shear stress that has to be overcome in order to fracture the field-induced particle structures in their weakest point, and thus to induce the flow of the material. This value of the shear stress, known as static yield stress, is the first parameter used to judge the strength of the MR effect in

magnetorheology.[5] The values of the static yield stress are usually estimated by plotting the rheograms in a double logarithmic scale (see Figures 6b and 6d), and then extrapolating the values of the shear stress corresponding to the low (around 0.1 s^{-1}) shear rate pseudoplateau to zero shear rate.[25] The obtained values of the static yield stress are plotted in Figure 7 as a function of the internal magnetic field for both nanosphere ferrofluid and nanofiber ferrofluid.
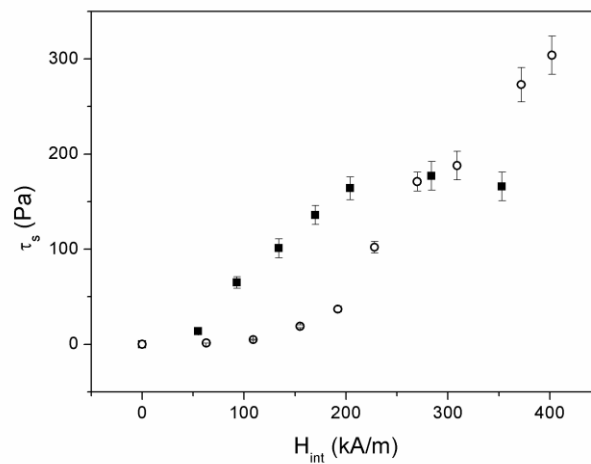

Figure 7. Static yield stress (τ_s) plotted as a function of the intensity of the internal magnetic field (H$_{int}$). Full squares represent the data for the ferrofluid composed of nanospheres; open circles the data for the ferrofluid composed of nanofibers.

It is interesting to note that the trends of the static yield stress are different for both ferrofluids. In the case of the nanosphere ferrofluid, the static yield stress presents a strong increase with the intensity of the magnetic field at low and medium field, and then saturates at not so high field values (H$_{int}$ > 200 kA/m). This MR trend, as well as the magnitude of the values of the static yield stress, is typical of suspensions of ferromagnetic spheres of slightly larger size –see for example the data for a MR fluid constituted by spherical particles with diameter 64 nm in Ref. 26. On the other hand, the magnetic field dependence of the static yield stress of the nanofiber ferrofluid is rather weak at low and medium field

($H_{int} < 100$ kA/m), and becomes very strong at higher field values. This difference in trends may be due to the existence of interparticle friction in the case of the nanofiber ferrofluid, and will be analyzed below in view of the proposed theoretical model. Regarding the magnitude of the yield stress of nanofiber ferrofluid with respect to nanosphere ferrofluid, it must be noted that the magnetic properties of the materials of both kind of particles are different, and the MR effect depends on these properties. As an example, the yield stress at saturation, τ_{sat}, is predicted to depend on the square of the saturation magnetization of the bulk material, M_b, (see Ref. 27), which is 742.5 kA/m and 626 kA/m for nanospheres and nanofibers respectively. Normalizing τ_{sat} by $\mu_0 M_b{}^2$ we obtain the following dimensionless static yield stress values at saturation: 2.6×10^{-4} for the nanosphere ferrofluid and 6.2×10^{-4} for the nanofiber ferrofluid. Thus we can conclude that the ferrofluid composed of nanofibers presents a stronger MR response than the ferrofluid composed of nanospheres. This result is in agreement with the stronger MR effect reported for MR fluids composed of microfibers as compared with conventional (based on spherical particles) MR fluids.[11-16] In fact, even the magnitude of the increment of τ_{sat} (2.4 times for nanofiber ferrofluid with respect to nanosphere ferrofluid) is in agreement with the 2-3 time increase reported for MR fluids composed of microfibers with respect to MR fluids composed of microspheres.[11]

4.2. The Bingham model. Dynamic yield stress and plastic viscosity

At high shear rate the $\tau - \dot{\gamma}$ relationships of Figure 6 appear to be linear, and can be well adjusted by the Bingham equation for shear stress:[28]

$$\tau = \tau_B + \eta_{pl}\dot{\gamma} \qquad (2)$$

In this equation τ_B is the dynamic (Bingham) yield stress and η_{pl} the plastic viscosity. The dependence of these two parameters on the magnetic field strength is also commonly analyzed as a way to quantify the MR response of MR fluids and ferrofluids. In the present work, these parameters were obtained by fitting equation 2 to the data of Figure 6 at $\dot{\gamma} > 25\,\mathrm{s}^{-1}$. The values of the dynamic yield stress are plotted as a function of the internal magnetic field in Figure 8.
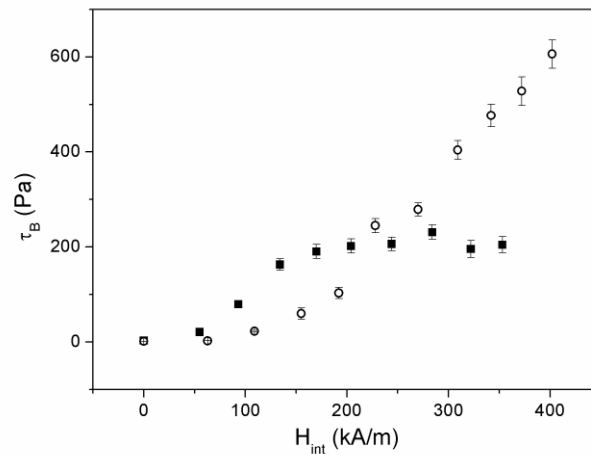

Figure 8. Dynamic (Bingham) yield stress (τ_B) plotted as a function of the intensity of the internal magnetic field (H$_{int}$). Full squares represent the data for the ferrofluid composed of nanospheres; open circles the data for the ferrofluid composed of nanofibers.

As it is observed, the trends obtained for the dynamic yield stress are similar to those seen in Figure 7 for the static yield stress, and indeed the same analysis could be drawn. The only remarkable difference between Figures 7 and 8 is the fact that the values of the dynamic yield stress (Figure 8) are higher than the values of the static yield stress (Figure 7). The reason for this difference can be found in the definitions of these yield stresses. As mentioned above the static yield stress is the shear stress required to induce the flow of a material. On the other hand, the dynamic yield stress is the one needed to continuously break the aggregates that reform in the presence of the magnetostatic forces.[25] These two

yield stresses have no reason for being equal, and actually the dynamic yield stress is usually higher than the static one, as it is the case of the present work.

Regarding the dependence of the plastic viscosity with the magnetic field strength (not shown here for brevity), similar trends to those observed in Figures 7 and 8 were also obtained, and a similar explanation applies too. However, the values of the plastic viscosity in the absence of applied field are worthy of attention. We obtained plastic viscosities in the absence of field of 54 ± 7 mPa·s for the nanosphere ferrofluid, and 62 ± 4 mPa·s for the nanofiber ferrofluid. We can compare these experimental values with theoretical predictions for the viscosity of suspensions. For the viscosity of the nanosphere ferrofluid Batchelor's formula can be used:[21]

$$\frac{\eta}{\eta_c} = 1 + 2.5\phi + 6.2\phi^2 \qquad (3)$$

η and η_c being the viscosities of the suspension and the carrier liquid, respectively, and ϕ the volume fraction of particles. Equation 3 holds good for suspensions of hard spheres up to $\phi \approx 0.10$. This equation gives a viscosity of 45 mPa·s for the nanosphere ferrofluid, whereas the experimental value is 54 ± 7 mPa·s. The difference is likely due to the existence of magnetostatic interactions between the particles (let us remember that they are single-domain particles), as well as to the deviation from spherical shape, which is clearly observed in Figure 1a. For the viscosity of the nanofiber ferrofluid the predictions for suspensions of spheroidal particles can be used.[29] With this aim, the fibers of the present work may be approximated by spheroids of high aspect ratio, p = 8.5. Upon this approximation we may use the following expression derived for suspensions of rigid spheroids at low shear rate:[21,29]

$$\frac{\eta - \eta_c}{\phi \eta_c} = \frac{4p^2}{15 \ln p} \tag{4}$$

This expression gives a viscosity of 57 mPa·s for the nanofiber ferrofluid, whereas the experimental value is 62 ± 4 mPa·s. As in the case of nanosphere ferrofluid, the difference is likely due to the existence of magnetostatic forces between nanofibers, as well as to the deviation from the spheroidal shape considered in the derivation of equation 4.

4.3. Magnetoviscous effect

In paragraphs 4.1 and 4.2 the MR response of ferrofluids has been analyzed through the values of the field-induced yield stress. However, in the case of ferrofluids it is more common to quantify their rheological response to applied magnetic fields through the magnetoviscous effect (MVE), which can be defined as:[30]

$$\mathrm{MVE} = \frac{\eta_H - \eta_0}{\eta_0} \tag{5}$$

Where η_H and η_0 are the viscosities of the ferrofluid at a given magnetic field (H) and at zero magnetic field, respectively. This dimensionless magnitude quantifies the *gain* in viscosity that can be reached at a given shear rate upon application of a magnetic field of certain strength. Actually, for most technological applications (e.g. MR dampers and bearings) this magnitude has more interest than the yield stress since the ferrofluid (or MR fluid) must work in the flow regime, where the yield stress is not relevant.
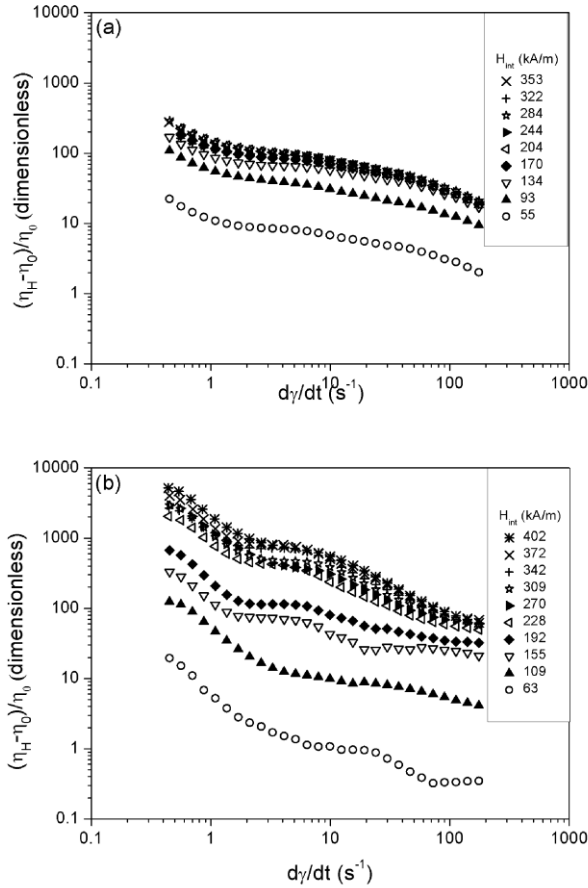
Figure 9. Magnetoviscous effect $\left(\dfrac{\eta_{\mathrm{H}} - \eta_0}{\eta_0} \right)$ plotted as a function of the shear rate ($\mathrm{d}\gamma/\mathrm{d}t$) for different intensities of the internal magnetic field (H_{int}). (a) Curves for the ferrofluid composed of nanospheres; (b) curves for the ferrofluid composed of nanofibers. Note that the scale of the axes is the same in both graphs.

In Figure 9 the MVE in the flow regime is plotted as a function of shear rate. As observed, the MVE presents a general trend to diminish with the shear rate for both ferrofluids and for all the intensities of the internal field. This is a logical tendency since as the shear rate is increased the particle aggregates are progressively destroyed, and thus their resistance to the flow regime diminishes too. It is noticeable, nevertheless, the difference in ranges of MVE that are obtained for nanosphere ferrofluid (Figure 9a) and for nanofiber ferrofluid (Figure 9b) –note that both graphs have the same scale in the axes. For nanosphere

23

ferrofluid the dependence of the MVE with shear rate is comparatively weak, and so it is the dependence with the magnetic field –the MVE is quickly saturated. On the other hand, the MVE depends strongly on the intensity of both the magnetic field and the shear rate for the nanofiber ferrofluid, and in spite of this a strong MVE is obtained even at the highest shear rate values.

This difference in behavior of the MVE for nanosphere ferrofluid and nanofiber ferrofluid is likely due to existence of solid friction between nanofibers, as it is the case for the yield stress. Besides, the anisotropic shape of nanofibers is expected to additionally contribute to the MVE, in particular at large shear rate where most of the aggregates are supposed to be broken, and thus interparticle friction is not expected to play a significant role. In order to explain this, let us suppose a large enough shear rate so that all the particles are free (not aggregated), and the magnetic field is not parallel to the direction of vorticity of the flow. Upon this assumption the hydrodynamic torque will force a misalignment of the magnetic moment of the particle and the magnetic field direction, which consequently will provoke the appearance of a restoring magnetic torque. Equilibrium between the hydrodynamic and magnetic torques will be reached at a certain angle of orientation between the magnetic moment of the particle and the magnetic field, and the free rotation of the particle in the flow will be prevented. This will increase the flow resistance of the ferrofluid and it is the base of the MVE in a regime of free (not aggregated) particles.[30] However, it is obvious that under these conditions the resistance of a nanofiber to the flow will be higher than the resistance of a nanosphere, and consequently, the MVE at large shear rate is also expected to be higher for the nanofiber ferrofluid than for the nanosphere ferrofluid. This is

corroborated in Figure 10, which shows the MVE at the highest shear rate considered in this work ($\dot{\gamma} = 175\,s^{-1}$), plotted as a function of the internal magnetic field strength.

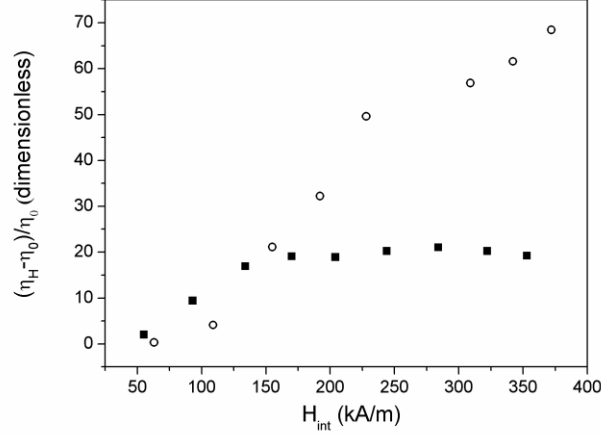Figure 10. Magnetoviscous effect $\left(\dfrac{\eta_{\mathrm{H}} - \eta_0}{\eta_0} \right)$ at $\dot{\gamma} = 175\,s^{-1}$, plotted as a function of the internal magnetic field strength (H_{int}). Full squares represent the data for the ferrofluid composed of nanospheres; open circles the data for the ferrofluid composed of nanofibers.

As observed, even in spite of its weaker magnetic properties (see sections 2 and 3), the nanofiber ferrofluid presents a stronger MVE than the nanosphere ferrofluid for almost all the intensities of the internal magnetic field. This corroborates the higher tunability of ferrofluids composed of nanofibers as compared to ferrofluids composed of nanospheres, which makes them more suitable for technological applications.

5. Theoretical model for the static yield stress

In this paragraph we propose theoretical models for the static yield stress of ferrofluids composed of spherical or fiber-like particles. Theoretical analysis of the rheological effects in the flow regime will be the subject of a future work.

5.1. Yield stress in ferrofluids composed of spherical particles

Elastic phenomena and yield stress effects in magnetic fluids appear due to the heterogeneous structures, consisting of magnetic particles, which span the channels in which the fluids flow. Two types of structures are the most commonly considered: linear chains and dense bulk drop- or column-like aggregates. Static elasticity of MR fluids (suspensions of magnetizable micron-sized particles) can be provided by both of these structures.[5] In the case of ferrofluids, the typical size of the particles (10-30 nm) is hundreds and even thousands of times smaller than the typical size of the flow channel. Therefore, the probability of appearance of a chain consisting of hundreds, not to say about thousands, of the ferrofluid particles is negligible. Thus the elastic and the static yield stress effects in ferrofluids can only be provided by the dense bulk columns, which appear as a result of the condensation phase transitions (gas-liquid or gas-solid) in ensembles of ferromagnetic particles.

A theory for the yield stress in magnetic fluids with dense column-like aggregates, spanning the flow channel, was developed in Ref. 31. It was shown that the elastic shear stress τ, which appears due to the inclination of the magnetic columns with respect to the applied magnetic field, is a non-monotonic (with a maximum) function of the static shear γ. If the applied shear stress exceeds the maximal magnitude τ_m of the elastic stress, the system cannot resist statically to the applied stress and begins to flow. Thus the static yield stress τ_y equals to τ_m. Another model for the transition of a magnetic fluid from the elastic to the flow regime was suggested in Ref. 27. The main idea proposed in this work is that the state of the column, inclined with respect to the applied field, is thermodynamically unfavorable. When the system shear γ exceeds some critical magnitude γ_c, separation of the

26

primary column into two "secondary" ones is thermodynamically favorable. The length of the secondary columns is supposed half of the length of the primary one. Thus, the length of the secondary column is smaller than the channel thickness. Therefore the secondary columns do not link the channel walls and thus they are not inclined with respect to the applied field. Separation of the column "bridges" between the walls into secondary shorter columns means the end of the sample elastic resistance to the applied stress. Thus the stress $\tau_c = \tau(\gamma_c)$ equals to the yield stress τ_y. Analysis performed in Ref. 27 shows that the first mechanism ($\tau_y = \tau_m$) of transition from the elastic deformation to the viscous flow is rather typical for suspensions constituted by micron-sized particles, i.e. for MR fluids. The second mechanism, when $\tau_y = \tau_c$, must be typical for magnetic fluids with particles about 10-40 nm in diameter, i.e. for ferrofluids. Since the mean diameter of the particles used in our experiments is about 24 nm, we believe that the yield stress phenomena in our systems must correspond rather to the second mechanism, i.e. to the mechanism of the "bridge" destruction, which consequently will be used here.

Let us consider a flat gap of thickness L, filled with a ferrofluid and placed in a magnetic field H_0 perpendicular to the gap walls. We suppose that the ferrofluid particles form dense ellipsoidal columns, which are domains of dense phase inside the ferrofluid. Because of the low total concentration of particles in the ferrofluid under study, and for the maximal simplification of the calculations, we will neglect the difference between the applied field, the external with respect to the sample, and the mean field inside the sample. At the beginning, the columns are aligned along the field direction. Then, let the gap be shifted in the wall plane. The elastic and yield stress effects can take place only in the case of strong binding between the column and the gap walls (no slipping of the column on the walls). Let

us assume the existence of strong binding. This is reasonable from the experimental viewpoint since the roughness of the rheometer plates is of the order of hundreds of nanometers and thus higher than the particle size. The primary and secondary columns are supposed highly elongated ($L \gg D_{1,2}$), where D_1 and D_2 are respectively the diameters of the primary and secondary columns. Like in Ref. 27, we suppose that the destruction takes place in the middle of the primary drops. The situation relative to drop separation is illustrated in Figure 11.
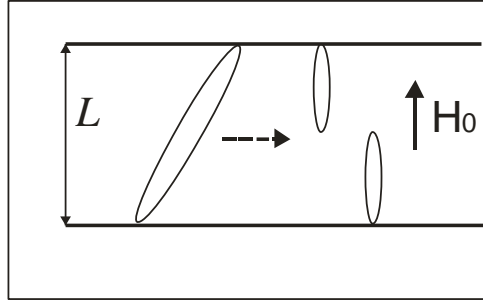

Figure 11. Sketch of the flow channel, with gap-spanning primary column (left), and the secondary ones (right).

Let us denote the gap wall shift as x. By definition the dimensionless shear strain of the system is $\gamma = x/L$. According to Ref. 27, the critical shear strain γ_c of the primary domain separation corresponds to equality among the free energy $F_1(\gamma)$ of the primary drop, and the total free energy F_2 of the two secondary drops. In other words, γ_c can be found from the condition $F_1(\gamma_c) = F_2$. The free energies F_1 and F_2 have been estimated in Ref. 27 taking into account the effect of the demagnetizing field of the highly elongated domain and the effect of the domain surface tension. However in Ref. 27 the mistake $S_2 \approx 2^{-1/2} S_1$ was made, S_1 and S_2 being the surface areas of the primary and secondary drops, respectively. The correct result is $S_2 \approx S_1/2$. By using the expressions derived in Ref. 27 for the free energies F_1 and F_2, and taking into account the correct relation between S_1 and S_2, we get:

$$\gamma_c \approx \sqrt{3K_1 \frac{2 + \chi_d}{1 + \chi_d K_1}} \tag{6}$$

Here, K_1 is the demagnetizing factor of the primary domain, and χ_d the magnetic susceptibility of the phase of this domain. The explicit form of K_1 can be determined if we model this domain by an ellipsoid of revolution. By using classical results for highly elongated domains we get:[32]

$$K_1 \approx c_1{}^2 \left| \ln c_1 \right|, \qquad c_1 = \frac{D_1}{L_1} \ll 1 \tag{7}$$

Here D_1 and L_1 are respectively the diameter and length of the primary domain. Then, according to Refs. 5,27,31, the quasielastic stress in the shifted gap with highly elongated domains can be presented as:

$$\tau(\gamma) \approx \frac{\mu_0}{2} \frac{\chi_d{}^2 H^2}{1 + \chi_d / 2} \frac{\gamma}{\left(1 + \gamma^2\right)^2} \Phi \tag{8}$$

Here μ_0 is the vacuum magnetic permeability, and Φ is the volume concentration of domains in the gap. Estimates show that the energy of magnetic interactions between the particles is much larger than the thermal energy kT in the ferrofluid under study. In this case almost all the particles must be condensed into the dense phase, i.e. in the domains; thus, their concentration out of the domains must be negligible. Taking it into account, we get easily that $\Phi = \dfrac{\varphi_0}{\varphi_d}$. Here φ_0 is the total hydrodynamic (taking into account the surfactant layers) volume concentration of magnetic particles in the ferrofluid, and φ_d their hydrodynamic concentration inside the domains of dense phase. In systems of strongly interacting particles φ_d is approximately equal to the dense packing concentration φ_m. For the maximal simplification of the calculations we model the ferrofluid as a monodisperse system of identical magnetic spheres. In order to estimate the domain susceptibility χ_d, we will use Langevin law:

$$\chi_d \approx 12\varphi_d \frac{\varepsilon}{\kappa} L(\kappa), \qquad L(\kappa) = \coth \kappa - \frac{1}{\kappa}, \tag{9}$$

$$\kappa = \mu_0 \frac{mH}{kT}, \qquad \varepsilon = \frac{\mu_0}{2\pi} \frac{m^2}{(d + 2s)^3 kT}$$

Here m is the magnetic moment of the particle, s the thickness of the surfactant layer adsorbed on its surface, d the diameter of the particle magnetic core, κ the dimensionless energy of the particle interaction with the magnetic field H, ε the dimensionless energy of

29

the magnetic interaction between two closely situated particles, and $L(\mathrm{x})$ is the Langevin function (do not confuse with the gap thickness). It should be noted that the magnetic interaction between the particles in the dense phase increases the domain susceptibility as compared with the prediction of Langevin law. However, taking this interaction into account will not change significantly the final results, but instead will lead to much more cumbersome calculations. This is the reason for which the susceptibility χ_d is determined here by using the simple Langevin law. In order to estimate the yield stress $\tau_y = \tau(\gamma_c)$ we should make use of equation 8, taking into account equations 6,7,9. For this aim, we should first determine the shape factor c_1, in order to estimate the demagnetizing factor K_1 of the primary domain by equation 7. According to Refs. 27,34, the following relation is held for this shape factor:

$$c_1 \approx \left(3\frac{\Lambda}{L\ln(L/\Lambda)}\right)^{1/3}, \qquad \Lambda = \left|\frac{\mu_0 W(1+\chi_d\Phi)}{4\mu_e HU\chi_d}\right| \qquad (10)$$

Here L is again the gap thickness, and μ_e the magnetic permeability of the dilute phase of ferrofluid, surrounding the dense domains. Since concentration of particles in this dilute phase is very low, as mentioned above, we may suppose that $\mu_e = \mu_0$. Parameters W and U appearing in equation 10 are determined as:[34]

$$W = \frac{v_{d\varphi}v_{e\varphi}}{Q}\sigma \qquad (11)$$

$$U = \frac{(v_{dH}-v_{eH})p_{e\varphi}-v_{e\varphi}(p_{dH}-p_{eH})}{Q}v_{d\varphi}+v_{dH}$$

where $Q = v_{e\varphi}p_{d\varphi} - v_{d\varphi}p_{e\varphi}$, and σ is the surface tension on the domain boundary. The magnitudes v and p mean the particle chemical potential and osmotic pressure respectively; indexes d and e relate to the dense domain and dilute environment respectively. The second indexes φ and H mean derivatives with respect to the particle volume concentration φ and magnetic field H, respectively –For example $v_{e\varphi} = \dfrac{dv_e}{d\varphi}$, and so on. These derivatives are determined at concentrations φ_e and φ_d in the dilute and dense phases of an infinite volume of the ferrofluid when the shape factor c_1 is negligible. According to general results of thermodynamics, the concentrations φ_e and φ_d satisfy the following system of equations:

$$v_e(\varphi_e) = v_d(\varphi_d) \tag{12}$$

$$p_e(\varphi_e) = p_d(\varphi_d)$$

The explicit forms of the functions $v_{e,d}(\varphi)$ and $p_{e,d}(\varphi)$ are given in Ref. 34. By using these explicit forms and under the assumptions that $\varphi_e \ll 1$, $\varphi_d \to \varphi_m$, the following solutions of the system of equations 12 are obtained:

$$\varphi_d \approx \varphi_m - \frac{A}{G\varphi_m}, \qquad \varphi_e \approx \exp(-G\varphi_m) \tag{13}$$

where $A \approx 2.2$ and $G \approx 2\varepsilon L^2(\kappa) + \frac{1}{3}\varepsilon^2$. Taking into account the explicit forms (see Ref. 34) for the chemical potentials v_e, v_d and the osmotic pressures p_e, p_d, and calculating their derivatives over φ and H at the concentrations given by equation 13, we obtain:

$$p_{e\varphi} \approx \frac{kT}{v}, \qquad p_{d\varphi} \approx \frac{kT}{v}G\varphi_m\left(G\frac{\varphi_m^2}{A}-1\right),$$

$$v_{e\varphi} \approx kT\exp(G\varphi_m), \quad v_{d\varphi} \approx kTG\left(G\frac{\varphi_m^2}{A}-1\right), \tag{14}$$

$$v = \frac{\pi}{6}\left(d+s\right)^3)$$

and

$$p_{eH} \approx -\alpha\frac{kT}{v}\varphi_e^2 G', \quad p_{dH} \approx -\frac{kT}{v}\alpha\varphi_d^2 G'$$

$$v_{eH} \approx -kT\alpha\left(L(\kappa)+2\varphi_e G'\right), \quad v_{dH} \approx -kT\alpha\left(L(\kappa)+2\varphi_d G'\right) \tag{15}$$

$$G' = \frac{dG}{d\kappa}, \qquad \alpha = \mu_0\frac{m}{kT}$$

According to Ref. 34, the surface tension σ can be estimated as:

$$\sigma \approx kTv^{-2/3}\varphi_d^2\varepsilon L^2(\kappa) \tag{16}$$

Combining equation 6 with equations 10,11, we come to the following expression for the parameter Λ:

$$\Lambda \approx \frac{1}{8}\left(\frac{\pi}{6}\right)^{1/3}\frac{(d+s)G}{12\varepsilon L(\kappa)(L(\kappa)+\varphi_m G')} \tag{17}$$

Finally, by combination of equation 17 with equations 6,7,10, the static yield stress of the ferrofluid constituted by spherical nanoparticles can be calculated by equation 8.

Results of our calculations are shown in Figure 12, along with the experimental data for comparison. As observed there is a reasonable quantitative agreement between theory and experiments. As a consequence, we may conclude that the considered mechanism of domain destruction, as well as the chosen criterion of this separation, is adequate to describe the experimental situation, at least, in their principal points.
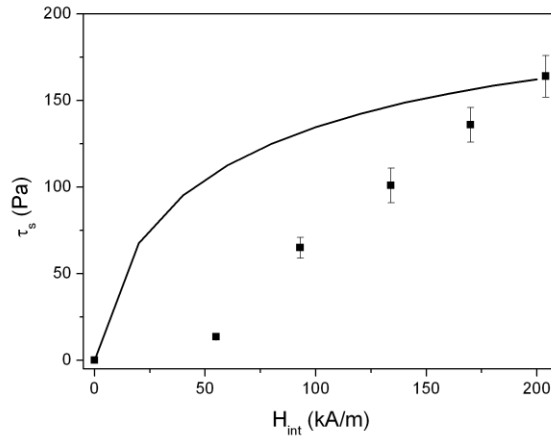

Figure 12. Static yield stress (τ_s) plotted as a function of the intensity of the internal magnetic field (H_{int}), for a ferrofluid composed of nanospheres (solid concentration 5 vol.%). Full squares represent the experimental data, and the solid line the theoretical data calculated by using equation 8 as described in the text.

5.2. Yield stress in ferrofluids composed of fiber-like particles

Previous investigations have shown that the contact friction between fiber-like microparticles plays a decisive role in the rheological properties and behavior of MR fluids.[12,35] We may expect that contact friction between fibers was also the reason for the obtained differences between the yield stress for the ferrofluid composed of nanofibers and

this composed of nanospheres –see Figure 7. The main qualitative difference between these experimental results for the yield stress is the different curvatures of the dependences of the yield stress τ_y on the magnetic field H (see Figure 7). The fact that for the system with the spheres the yield stress comes to saturation is not surprising. Indeed, in the region 100 kA/m < H < 200 kA/m for these systems the dimensionless field κ is much more than unity. Therefore, magnetization of the dense domains of spheres in this region comes to saturation, which means the saturation of the yield stress.

The measured dependence of the yield stress on the field for the ferrofluid composed of fibers is also quite typical at low field (H < 100 kA/m), when the domains susceptibility χ_d is approximately constant. On the other hand, estimations show that for the fibers the dimensionless parameter κ in the region of the field 100 kA/m < H < 400 kA/m is also much more than unity. Consequently, if in these measurements the internal state of the domains had been thermodynamic equilibrium, the field dependence of the yield stress would have been qualitatively the same negative curvature as for the system with spheres. Thus, the detected positive curvature of the function $\tau_y(H)$ (see Figure 7) indicates that during the measurements the internal state of the dense domains was far from equilibrium. One can suppose that the reason for this is the strong friction between the fiber-like particles in the domains.

In this part of the work we suggest a simple phenomenological model for the yield stress in a system with strong interparticle friction. According to the results shown in section 3, we may assume that the nanofiber ferrofluid is in a concentrated isotropic regime, in which the nanofibers begin to have difficulty packing isotropically. As a consequence, when the magnetic field is switched on, a perfect alignment of the individual nanofibers with the

field is likely impossible due to the contact (friction) forces between them and, thus, the resulting field-induced structures likely consist of entangled networks of nanofibers. We will consider each field-induced structure as a domain with very high concentration of nanofibers. We will also consider that, because of the existence of interparticle friction, the magnetic moment of a domain does not change after the sample shift induced by the shear, being always aligned along the domain axis. Let us denote by M_d the magnetization of the domain under the field H, and with ψ the angle between the domain axis and this field. The following relation $\gamma = tg\,\psi$ is held. According to considerations of Ref. 31, we can determine the elastic stress in the gap as:

$$\tau = -n_d\,\frac{\partial F_d}{\partial \gamma} \tag{18}$$

where n_d is the number of domains per unit volume of the sample, and F_d is the change of free energy of the domain due to its inclination from the field. Under the assumptions that the magnetic moment of the domain does not change while the sample is shifted, and that it is always aligned along the domain axis, we get:

$$F_d = -\mu_o M_d V_d H \cos\psi = -\mu_0 M_d V_d H \frac{1}{\sqrt{1+\gamma^2}} \tag{19}$$

Here V_d is the volume of the domain. Substituting equation 19 into equation 18 and taking into account that $n_d V_d = \Phi$, where Φ again is the volume concentration of domains, we get:

$$\tau = \mu_0 M_d H \frac{\gamma}{\left(1+\gamma^2\right)^{3/2}} \Phi \tag{20}$$

The concentration Φ again can be estimated as $\Phi = \varphi_0/\varphi_d$, where φ_0 and φ_d are the total volume concentration of nanofibers in the ferrofluid and inside the domain respectively.

The problem now is the estimation of the domain magnetization M_d taking into account the friction forces between particles. Obviously, this problem cannot be strictly solved. In order to get, at least, a qualitative description of the system, we use some variant of the mean field approximation. Let us consider a ferromagnetic fiber placed into a medium and interacting with this medium through dry friction forces. In this model the contact interaction of a particle with the other particles is approximated by the friction interaction of the particle with the effective medium. We assume that before the field is switched on, the particles have a random orientation. Therefore, the mean magnetic moment of such an ensemble of particles is zero. This assumption corresponds to the experimental situation.

Let θ be the angle between the fiber magnetic moment and the applied magnetic field. Taking into account the dry friction interaction between the particle and the effective medium, the equation of particle rotation, under the field action, can be presented as:

$$\beta \frac{d\theta}{dt} = \begin{cases} -\mu_0 mH \sin\theta + \xi, & |\mu_0 mH \sin\theta| \geq \xi \\ 0, & otherwise \end{cases} \qquad (21)$$

In the spherical coordinate system $0<\theta<\pi$, and thus $\sin\theta \geq 0$. Here m is again the particle magnetic moment, ξ is the critical torque for particle rotation, determined by its dry friction with the medium, i.e. by the contact interaction of the particle with the other ones; and β is the coefficient of the viscous friction of the particle with the medium. Note that if $\xi=0$ (dry friction is absent) equation 21 coincides with the well known equation of rotation of a ferromagnetic particle under the action of a magnetic field H. Determination of the friction parameter ξ requires a detailed analysis of the particle contacts and the friction in these contacts. Obviously, this represents a very difficult and cumbersome problem. Here we will

consider ξ as an empirical parameter. We are interested in the equilibrium orientation of the particle, which is determined by the angle θ_1 that satisfies the following equation:

$$\sin \theta_1 = \frac{\xi}{\mu_0 mH} \qquad (22)$$

It follows from equation 21 that only the particles with an initial angle satisfying the condition $\sin \theta > \sin \theta_1$, can rotate upon field application and achieve the position with the angle θ_1. Particles with an initial angle for which $\sin \theta < \sin \theta_1$, cannot rotate upon magnetic field application because of the friction. These particles do not contribute to the domain magnetization. Let φ_d be the total volume concentration of particles in the phase of the dense domain. Simple geometrical considerations show that the volume concentration of particles that are able to rotate upon field application, and achieve the position with angle θ_1, is (see illustration in Figure 13):

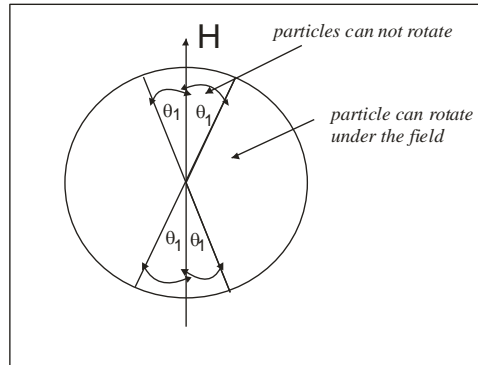$$\varphi_1 = \varphi_d \left(1 - \frac{2}{\pi} \theta_1 \right) \qquad (23)$$

Figure 13. Illustration of the angle distribution of particles that can rotate under the applied field and that cannot rotate.

If a particle is inclined from the field H at the angle θ_1, its magnetic moment component along the field is $m_H = m\cos\theta_1$. Taking it into account, as well as the concentration of the inclined particles, given by equation 23, we come to the following estimation for the magnetization of the dense domain phase:

$$M(\xi) = m\frac{\varphi_d}{v_f}\cos\theta_1\left(1 - \frac{2}{\pi}\theta_1\right) \tag{24}$$

Here v_f is the volume of a fiber-like particle. Equation 24 has been obtained under the assumption that the dry friction torque is identical for all the particles. However, this is not the case for real systems. Obviously, the different particles have a different number of contacts with the other particles, and thus different mutual dispositions, which determine the friction interaction, etc. Thus, some statistical distribution over the magnitude of ξ must be considered. Precise determination of this distribution requires a special study and, at this moment, we do not have enough information to determine it quantitatively. Because of this reason, the present analysis will be restricted to a qualitative one and we will assume that the distribution function has a Gaussian form:

$$f(\xi) = \frac{\exp\left(-\dfrac{(\xi - \xi_0)^2}{\beta^2}\right)}{\displaystyle\int_0^\infty \exp\left(-\dfrac{(\xi - \xi_0)^2}{\beta^2}\right)d\xi} \tag{25}$$

Here ξ_0 is the mean magnitude of ξ, and β is dispersion of this distribution. Then, the mean magnetization of the dense phase can be determined as:

$$M_d = \int_0^\infty M(\xi)f(\xi)d\xi \tag{26}$$

Substituting equation 26 into equation 20 we estimate the elastic stress τ as a function of the shear γ. One may suppose that the strong friction, dominating over the particles Brownian motion, does not allow the destruction of the domains into two secondary columns, not even at very high deformation. Thus, now the transition from the elastic to the flow regime rather corresponds to the maximum of the function $\tau(\gamma)$. This maximum takes place when $\gamma = \gamma_m = 1/\sqrt{2}$. Therefore we get:

$$\tau_y = \tau(\gamma_m) = \frac{2}{3^{3/2}} \mu_0 M_d H \Phi \qquad (27)$$

Taking into account the estimation of M_d (equation 26) and that $\Phi = \varphi_0/\varphi_d$, it is found that the yield stress (equation 27) does not depend on the concentration φ_d of the particles in the domain. Figure 14 illustrates the results of the calculations of the yield stress.
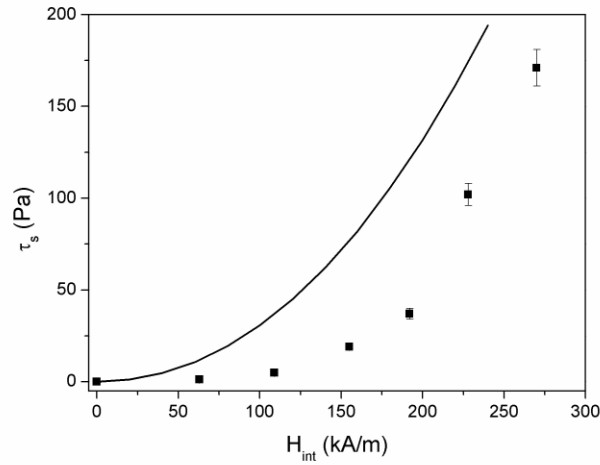

Figure 14. Static yield stress (τ_s) plotted as a function of the intensity of the internal magnetic field (H_{int}), for a ferrofluid composed of nanofibers (solid concentration 5 vol.%). Full squares represent the experimental data, and the solid line the theoretical data calculated by using equation 27 as described in the text. Parameters of the system: $\xi_0 = \mu_0 \dfrac{m^2}{v_f}$, $\beta = 1.5\xi_0$.

Note that, as any mean-field theory, our model does not allow to predict the magnitudes of parameters ξ_0 and β, which must be considered as empirical. Nevertheless, the proposed model describes correctly the curvature of the function $\tau_y(H)$. Besides, for reasonable magnitudes of these parameters it leads to a quite good agreement with experiments, as observed in Figure 14. The proposed theory shows that, unlike to ferrofluids composed of nanospheres where the contact friction between particles is practically negligible, in ferrofluids composed of fiber-like particles interparticle friction seems to play a decisive role in the development of the static yield stress.

6. Conclusions

Two new kinds of ferrofluids have been presented and their rheological properties upon magnetic field application have been thoroughly studied from the experimental viewpoint. The common feature that differences these ferrofluids from a conventional one (based on nanospheres of approximately 10 nm in diameter) is their larger particle size –besides, one of them is composed of fiber-like particles instead of spherical ones. The larger particle size, 24 nm in diameter for nanospheres and 56 nm in length × 6.6 nm in width for nanofibers, has proved to be an advantage from the point of view of the intensity of the MR effect. The reason for this is that these particles, although small enough to be magnetically single-domain and superparamagnetic, are large enough to make the magnetostatic forces dominate over the Brownian motion. As a consequence, they develop large yield stresses and viscosities upon field application. Because of the same mentioned reason, the stability of these new ferrofluids is worse than that of conventional ferrofluids, in which Brownian motion prevents from particle irreversible aggregation. Nevertheless, these new ferrofluids

with properties intermediate between those of conventional ferrofluids and MR fluids could be good candidates for applications in which fluids with moderate MR effect and stability are required.

Concerning particle shape, we have found interesting effects on the rheological behavior of the ferrofluids. A first difference has been found in the shape of the rheograms (Figure 6) obtained upon field application, which show a typical plastic behavior in the case of ferrofluids based on nanospheres, but present an unexpected N-like shape for ferrofluids based on nanofibers. This N-shape dependence is likely due to the existence of contact friction between fibers, which is expected to prevent from the destruction of the field-induced, percolating aggregates up to a critical value of the shear rate. When this critical value is achieved, these aggregates are destroyed and, consequently a strong decrease of the measured shear stress should take place. We may assume some statistics on the distribution of the initial percolating aggregates over friction, which will give rise to a smooth decrease of the shear stress, as observed in our experiments. Besides, we have found that fiber-like particles give rise to a stronger MR effect, evidenced in the magnitude of both the yield stress and the viscosity upon field application of the corresponding ferrofluid. Nevertheless, the most intriguing difference is on the curvature of the yield stress vs. magnetic field curve (Figures 7 and 8). In the case of the ferrofluid based on nanospheres, this curve presents a negative curvature, with the expected saturation of the yield stress at medium-high field. However, in the case of the ferrofluid based on nanofibers, the curvature is positive, increasing the yield stress faster the higher the applied field, without reaching saturation at the highest applied field.

We have developed theoretical models for the static yield stress of the ferrofluids. The rheograms of the ferrofluids based on spherical particles (Figure 6a) are well determined by the existence of bulk dense drop-like structures, which provide the static quasielastic deformation and the yield-stress phenomena in these systems. Size of these drops continuously decreases with the shear rate, leading to the observed monotonic dependence of the shear stress on shear rate. Results of the theoretical analyses have shown that in ferrofluids based on spherical particles the static yield stress is determined by the destruction of the primary domains of dense phase into secondary drops that align along the field. In ferrofluids based on fibers, interparticle contact friction is expected to play a decisive role in the determination of the static yield stress and the viscous stress in the flow regime. As it is the case for nanosphere ferrofluids, the static quasi elastic deformation of the nanofiber ferrofluids is determined by the existence of bulk aggregates (drops), consisting of the magnetic particles. In this case (nanofiber ferrofluids), interparticle friction hinders remagnetization and the consequent achievement of the thermodynamically equilibrium magnetization of the drops after application of the magnetic field. This leads to the experimentally observed positive curvature of the yield stress vs. magnetic field curve, even at magnetic fields for which systems in thermodynamical equilibrium will achieve saturation of the drop magnetization and, therefore, of the yield stress.

Acknowledgements

References

(1) Rosensweig, R. E. *Int. Sci. Tech.* **1966**, (July), 48-56.

(2) Rosensweig, R. E. *Ferrohydrodynamics*, Cambridge University Press: New York, 1985.

(3) Papell, S. S. *Low viscosity magnetic fluid obtained by the colloidal suspension of magnetic particles*, U.S. Patent 3,215,572; 1965.

(4) Rabinow, J. *AIEE Trans*. **1948**, 67, 1308-1315.

(5) Bossis, G. ; Volkova, O.; Lacis, S.; Meunier, A. *Lect. Notes Phys.* **2002**, 594, 201-230.

(6) Park, B. J.; Fang, F. F.; Choi, H. J. *Soft Matter* **2010**, 6, 5246-5253.

(7) Shliomis, M. I. *Sov. Phys.-Usp.* **1974**, 17, 153-169.

(8) Ilg, P.; Odenbach, S. *Lect. Notes Phys.* **2009**, 763, 249-325.

(9) Pop, L. M.; Odenbach, S. *J. Phys.-Condes. Matter* **2006**, 18, S2785-S2802.

(10) Zubarev, A. Y.; Iskakova, L. Y. *Physica A* **2007**, 376, 38-50.

(11) López-López, M. T.; Vertelov, G.; Kuzhir, P.; Bossis, G.; Durán, J. D. G. *J. Mater. Chem.* **2007**, 17, 3839–3844.

(12) López-López, M. T.; Kuzhir, P.; Bossis, G. *J. Rheol.* **2009**, 53, 115-126.

(13) Bell, R. C.; Karli, J. O.; Vavreck, A. N.; Zimmerman, D. T.; Ngatu, G. T.; Wereley, N. M. *Smart Mater. Struct.* **2008**, 17, 015028.

(14) Bell, R. C.; Zimmerman, D.; Wereley, N. M. In *Electrodeposited Nanowires and Their Applications*; Lupu, N., Ed.; Intech: Vienna, 2010; Chap. 8, pp. 189–212.

(15) Kuzhir, P.; López-López, M. T.; Vertelov, G.; Pradille, C.; Bossis, G. *Rheol. Acta* **2008**, 47, 179-187.

(16) De Vicente, J.; Segovia-Guitérrez, J. P.; Anablo-Reyes, E.; Vereda, F.; Hidalgo-Alvarez, R. *J. Chem. Phys.* **2009**, 131, 194902.

(17) Shahnazian, H.; Graf, D.; Borin, D. Y.; Odenbach, S. *J. Phys. D-Appl. Phys.* **2009**, 42, 205004.

(18) Gómez-Ramírez, A.; López-López, M. T.; Durán, J. D. G.; González-Caballero, F. *Soft Matter* **2009**, 5, 3888–3895.

(19) Herpin, A. *Théorie du Magnétisme*, Bibliothèque des Sciences et Techniques Nucléaires: Paris, 1968; pp. 749-754.

(20) O'Handley, R. C. *Modern Magnetic Materials: Principles and Applications*, John Wiley & Sons: New York, 2000; p. 305.

(21) Larson, R. G. *The Structure and Rheology of Complex Fluids*, Oxford University Press: New York, 1999; pp. 263-323.

(22) López-López, M. T.; Kuzhir, P.; Durán, J. D. G.; Bossis G. *J. Rheol.* **2010**, 54, 1119-1136.

(23) Laun, H. M.; Schmidt, G.; Gabriel, C.; Kieburg, C. *Rheol Acta* **2008**, 47, 1049–1059.

(24) Meeker, D.C. Finite Element Method Magnetics, Version 4.2 (15Jul2009 Mathematica Build), http://www.femm.info

(25) Volkova, O.; Bossis, G.; Guyot, M.; Bashtovoi, V.; Reks, A. *J. Rheol.* **2000**, 44, 91–104.

(26) López-López, M. T.; Kuzhir, P.; Meunier, A.; Bossis, G. *J. Phys.-Condes. Matter* **2010**, 22, 324106.

(27) Zubarev, A. Y.; Iskakova, L. Y. *Physica A* **2006**, 365, 265-281.

(28) Friend, J. P.; Hunter, R. J. *J. Colloid Interface Sc*i. **1971**, 37, 548-556.

(29) Hinch, E. J.; Leal, L. G. *J. Fluid Mech.* **1972**, 52, 683-712.

(30) Odenbach, S.; Thurm, S. *Lect. Notes Phys.* **2002**, 594, 186-201.

(31) Bossis, G.; Lemaire, E.; Volkova, O.; Clercx, H. *J. Rheol.* **1997**, 41, 687-704.

(32) Landau, L. D.; Lifshitz, E. M. *Electrodynamics of Continuous Media*, Pergamon: New York, 1984.

(33) Buyevich, Y. A.; Zubarev, A. Y. *J. Phys. II France* **1993**, 3, 1633-1645.

(34) Zubarev, A. Y.; Iskakova, L. Y. *Physica A* **2006**, 367, 55-68.

(35) Kuzhir, P.; López-López, M. T.; Bossis G. *J. Rheol.* **2009**, 53, 127-151.

Table of Contents Graphic

MAGNETIC FLUIDS CLASSIFICATION